Spring 5-1-2016

Stability Of Norwalk Virus Capsid Protein Interfaces Evaluated By In Silico Nanoindentation

Prakhar Bansal
University of Connecticut, prakharbansal2012@live.com

STABILITY OF NORWALK VIRUS CAPSID PROTEIN INTERFACES EVALUATED BY IN SILICO NANOINDENTATION

Author: Prakhar Bansal

Research Advisor: Eric May

Honors Advisor: Eric May

University Scholar Committee: Eric May (chair), Victoria Robinson, Carolyn Teschke

University of Connecticut

Department of Molecular and Cell Biology

Abstract

Studying the mechanical properties of viral capsids can give several insights into not only the lifecycle of the virus, but also into potential drug targets to thwart the progression of viral infection. Nanoindentation using an atomic force microscope is a useful technique for determining structural properties of small molecules and particles, and is commonly used to study viral capsids. This technique utilizes the probe of the microscope to push down on the capsid and record the forces along the indentation path. We ran this experiment *in silico* where we simulated the nanoindentation of Norwalk virus capsids using molecular dynamics. Running a simulation of the nanoindentation allowed us to observe the capsid deformation in much more detail than is possible experimentally. We were able to identify a distinctly weak interface in the Norovirus capsid. This interface might be the initial interface to disassemble during viral uncoating in the host cell for infection to proceed. Strengthening this interface might prevent uncoating and further infection. We identified three sites in this weak interface that may prove to be good drug targets for an antiviral treatment of Norwalk virus. Our study culminated in a publication in the journal Frontiers in Bioengineering and Biotechnology (Boyd, K. J., Bansal, P., Feng, J., & May, E. R. (2015). Stability of Norwalk Virus Capsid Protein Interfaces Evaluated by in Silico Nanoindentation. Frontiers in Bioengineering and Biotechnology, 3(July), 1–8. doi:10.3389/fbioe.2015.00103).

Introduction

Norwalk virus (genus *Norovirus*) is the leading cause of gastroenteritis worldwide[1]. Norovirus outbreaks commonly occur in settings with high levels of contact and less-than-ideal hygiene such as hospitals and nursing homes, cruise ships, and schools. In otherwise healthy populations, Norwalk virus is generally mild, and self-limiting, but there is evidence to support that it can lead to future illnesses, and can be fatal for the elderly and otherwise immunocompromised[2]. It is estimated by the World Health Organization as the most common cause of death from foodborne diarrhea disease and the fourth greatest burden in terms of disability-adjusted life years[3]. In the United States, noroviruses are responsible for about 20 million cases annually, leading to an average of 70 000 hospitalizations and up to 800 deaths every year[4]. The virus is particularly devastating in developing countries where it is estimated to cause over 212 000 deaths annually[3], with 70 000 of those being children[5]. There are currently no vaccines or specific anti-viral therapies for Norwalk virus[6], and treatment is limited to rehydration (in order to alleviate the mal-effects of diarrhea)[2]. This is largely attributed to the critical knowledge gaps about the virus.

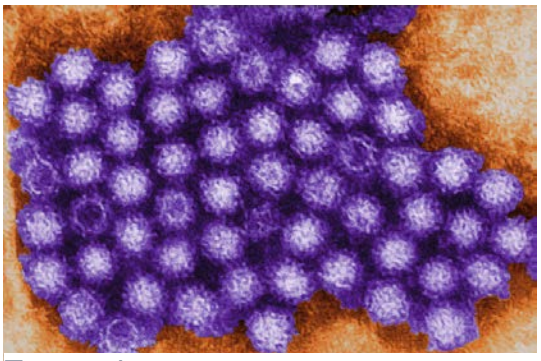

FIGURE 1
A transmission electron micrograph of Norovirus particles. (Photo Credit: Charles D. Humphrey, Centers for Disease Control and Prevention. http://www.cdc.gov/media/subtopic/library/diseases.htm)

There is very little known about the basic epidemiology of Norovirus in developing countries[3]. Norovirus is predominantly spread person-to-person[5], but there is a limited understanding of the role of different age groups in virus transmission[3]. Foodborne transmission is only responsible for about 15% of the transmission[5]. Individuals living in settings with poor sanitation and hygiene (as in developing

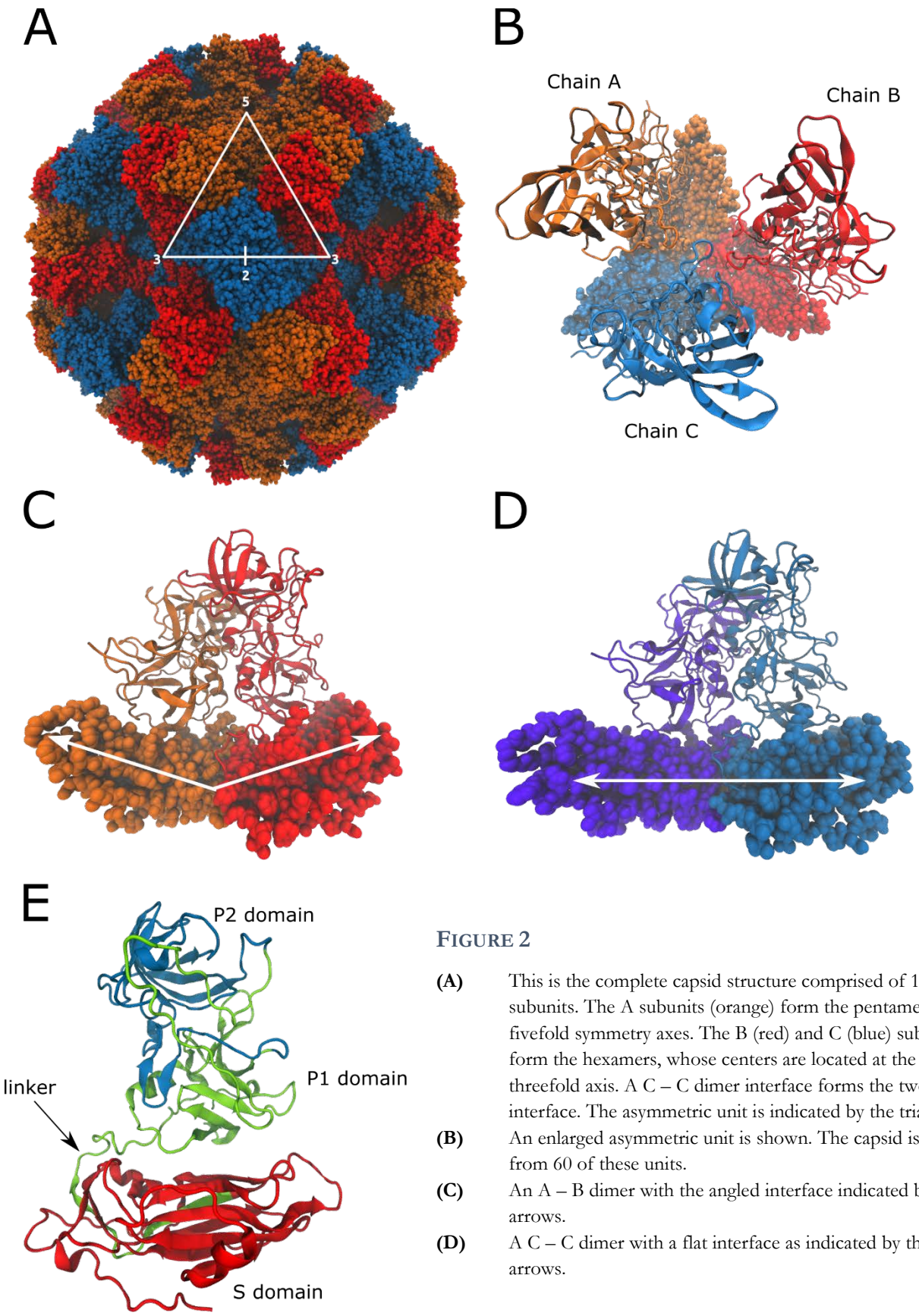

FIGURE 2

(A) This is the complete capsid structure comprised of 180 VP1 subunits. The A subunits (orange) form the pentamers at the fivefold symmetry axes. The B (red) and C (blue) subunits form the hexamers, whose centers are located at the threefold axis. A C – C dimer interface forms the twofold interface. The asymmetric unit is indicated by the triangle.

(B) An enlarged asymmetric unit is shown. The capsid is made from 60 of these units.

(C) An A – B dimer with the angled interface indicated by the arrows.

(D) A C – C dimer with a flat interface as indicated by the arrows.

countries) are more likely to be exposed to norovirus from multiple sources[5], and poor health care and availability to clean water makes treatment of symptoms more difficult.

The matter of vaccine development is complicated by evidence that supports the need for a polyvalent vaccine against norovirus due to its antigenic variation[3]. Much like the seasonal flu vaccine, this would require the synthesis of an updated vaccine when new pandemic strains of the virus emerge[3]. The rapid mutation of Norovirus makes vaccines increasingly impractical[7]. An antiviral therapeutic, however, may be useful in preventing the rapid spread of the disease in isolated and crowded settings like cruise ships.

The human norovirus is a small (~38 nm in diameter), icosahedral non-enveloped virus. It has a positive-sense single stranded RNA genome with three genes: ORF1, ORF2, and ORF3. ORF2 encodes the norovirus major capsid protein VP1. When ORF2 is expressed in insect cells, the VP1 that is produced self-assembles into Norwalk Virus-Like Particles (NVLPs). These NVLPs are morphologically and antigenically similar to native norovirus[1]. This allows NVLPs to be studied as a suitable substitute for human norovirus as they are easy to produce in large quantities, and are not infectious due to the lack of genetic material. We are using the 3.4 Å resolution NVLP structure determined via X-ray crystallography for our study[8].

The Norwalk virus capsid exhibits $T = 3$ icosahedral symmetry. It consists of 180 individual VP1 proteins. The VP1 protein has two domains: the shell (S) domain, and the protruding (P) domain. The S domain makes up the spherical body of the capsid, and the P domain creates arc-like structures that extend outwards from the capsid surface at every twofold line of symmetry. The P domain is made of two subdomains: P1, and P2[9]Figure 2. A flexible hinge connects the S and P domains (shown in Figure 2). It has been shown that the S domain alone is enough to assemble the actual capsid. A mutant VP2 with its P domain deleted was able to form a capsid (CT303) that

resembled the wild type NVLPs without the protruding domains[1]. This suggests that the S domain is sufficient for the assembly of the icosahedral capsid. The P domain has been found to be critical in several structural dynamics of the Norwalk virus capsid. It has a role in increasing the capsid rigidity[9], and in mediating host cell attachment[10,11]. Since the P domain is somewhat flexible, it is able to recognize and bind to several different host antigens[10,11]. This adds to the pervasive infectivity of the virus and makes it much harder to create preventative treatments.

In order to form the icosahedral capsid, the VP1 protein assumes three quasi-equivalent conformations[12], conventionally referred to as A, B, and C[1] (Figure 2 A-B). The capsid assembles from VP1 dimers. In the capsid, these dimers exist in two distinct conformations, and can be distinguished as A-B dimers and C-C dimers. The C-C dimers exist in a relaxed conformation analogous to the dimer configuration in free solution (Figure 2 D). In contrast, the A-B dimer conformation is slightly strained due to their placement in the capsid (Figure 2 C). This can be seen in the relatively linear interface between the C-C dimer, and the slightly angled interface between the A-B dimer.

Viral entry proceeds through endocytosis by the host cell through a non-clathrin, non-caveolin mechanism[13]. Once inside the host cell, the virus needs to expose its RNA to the cytoplasm where it can be translated, and the virus can be replicated. Little is known about the uncoating process through which this happens, but since the capsid does not have pores, the uncoating process is thought to involve a partial or complete disassembly of the capsid. An understanding of the mechanical strength of the various interfaces in the capsid may lend insights into requirements for disassembly.

Atomic force microscopy (AFM) indentation experiments have been performed on NVLPs to gain insights into the mechanical properties of the capsid. In these experiments, the viral particle is

adhered to a slide, and can either be kept in liquid solution or air for the duration of the experiment. In imaging mode, the tip of the AFM is able to scan the surface of the NVLP, and produce a topographical image. This allows for measurements of the size of the capsid. In indentation mode, the AFM tip can be used to apply a controlled force on the capsid. As the indentation progresses, the amount of force (F) and distance (Z) is recorded in what is known as an FZ curve. These measurements can provide information about the strength and flexibility of the entire capsid. The FZ curve typically has an initial linear slope that yields the particle's 'spring constant'. This is followed by a sharp drop that correlates to the buckling or fracture of the shell[14]. The location of this drop gives the critical force and indentation at which capsid failure occurs.

There have been two nanoindentation experiments done on Norwalk virus to date. The first focused on the influence of pH on the mechanical behavior of the capsid[15]. In that work, when the experiments were performed under neutral pH, the measured spring constant was 0.05 N/m. In this study, however, the measured capsid dimensions were inconsistent with the known dimensions. This may indicate that the particles may have been deformed in the preparation or imaging mode leading to an inaccurate stiffness. A second study that examined the influence of the P domain on the mechanical properties of NVLPs found the wild-type NVLP to have a spring constant of 0.30 N/m[9]. Their capsid dimensions were consistent with the known values, and so we were inclined to use their values for further referencing.

Our goal in this study was to perform nanoindentation simulations on the NVLP in order to obtain information that cannot be observed through AFM experiments. It has been demonstrated that simulations can reasonably reproduce nanoindentation experiments. In fact, a simulation study utilizing a coarse grained model was able to measure the spring constant of 35 capsids with good agreement for systems with known spring constants[16]. Furthermore, the incredible resolution of

computational studies can give unique insights into the structure and dynamics of biological machines. For example, in a typical (non-simulated) nanoindentation experiment, there is no way to calculate intermolecular forces during the capsid deformation, but this can be done easily through computational simulation of the system.

Specifically, we wish to obtain information about the relative strengths of the various protein-protein interfaces in the Norwalk virus capsid. This may provide insights into the mechanisms of uncoating, which could be used for development of antivirals that work by inhibiting this uncoating process[17].

Methods

Overview of Molecular Dynamics

In the *Feynman Lectures on Physics*, it is stated[18] that "everything that living things do can be understood in the jigglings and wigglings of atoms". Molecular dynamics (MD) is an attempt to study the dynamics of macromolecules, such as proteins, nucleotides, lipid bilayers, and carbohydrates[19], by examining this seemingly random movement of atoms. This is done by integrating the classical Newtonian equations of motion for all the atoms in a system[19]. These equations are integrated at very small time steps (typically 2 fs), several million times to get an adequate amount of simulation data. At present, it is common to see total simulation trajectories that are several hundred nanoseconds, or even microseconds long. Once the motion of the system is known, several structural and dynamic properties can be determined for the molecule.

Each calculation is done to determine the various microstates in the system throughout the trajectory. The microstate of each particle i is defined as a function of its position r_i and momentum

p_i called the Hamiltonian H. This function is a sum of the kinetic energy K and the potential energy V[19].

$$H(r,p) = K(p) + V(r) \quad (1)$$

The kinetic energy takes a familiar form that depends on m_i (the mass of particle i) and p_{ix}, p_{iy}, p_{iz} (the x, y, z components of its momentum p)[19].

$$K = \sum_{i=1}^{N} \frac{1}{2m_i}\left(p_{ix}^2 + p_{iy}^2 + p_{iz}^2\right) \quad (2)$$

The potential energy V is much more difficult to calculate and generally has to be estimated. In MD, the potential energy function V is given as a force field, and is the sum of various interactions. There are a variety of force fields that can be used such as AMBER[20], CHARMM[21], GROMOS[22], and OPLS[23]. Generally, the potential energy is divided into two parts in these force fields: the bonded terms (comprised of bond, angle, dihedral, and improper interaction terms), and the non-bonded terms (comprised of Van der Waals (vdW) and electrostatic interaction terms)[19].

$$V = V_{bond} + V_{angle} + V_{dihedral} + V_{improper} + V_{vdw} + V_{elec} \quad (3)$$

These terms address the different forces that may be acting on the particle at each time-point. These interactions are calculated pairwise for all the atoms in the system. Generally, the bonded terms are easier to compute than the non-bonded terms because they involve smaller pairs of atoms. In contrast, a non-bonded interaction like Van der Waals can involve long range interactions that involve all the atoms in the system. For this reason, there is generally a cutoff distance defined for long range interactions to speed up the calculation. There are several other optimizations that are made to simplify many of these calculations to make them easier to compute. Even after these optimizations, simulations take a very long time to compute even on large computational clusters.

For a large system such as a viral capsid, further simplification of the system is often necessary to get meaningful lengths of simulations.

Coarse Graining via a Gō Model

We are using a modified coarse grained Gō model for the viral capsid [insert citation for Eric May's paper]. A coarse grain model is necessary for the indentation simulations because the viral capsid is too large a system to simulate at an atomistic level given the resources we have. A Gō model is especially good for looking at protein dynamics.

The general scheme for creating a coarse-grained (CG) Gō model is that the atoms for each residue are grouped into a single bead. Then there is a force field created based the "master contacts" in the initial structure. A contact is defined when a pair of residues have a minimum distance of 12 angstroms or less in the initial atomistic structure. These initial distances for the contacts are favored throughout the length of the simulation. An attractive force is felt between contact pairs. This sort of model is well suited for our indentation simulation as it focuses the calculation on the deforming forces on the protein, which is our parameter of interest. It can help us study the deformation of the large viral capsid system in a much more computationally simplified way. It allows our simulations to complete in a matter of weeks, rather than years.

As a part of this project, we also wanted to generalize our method of making Gō models of viral capsids, as the current scripts are labor intensive and time consuming methods and require manual intervention in making these models. The process was fully automated using original software created by me.

We can run CHARMM Gō Model Builder to get a structure and native contacts for an expanded asymmetric unit. This model also includes non-bonded forces between neighboring asymmetric units, but it is challenging to map these neighboring contacts to the right neighbors for each of the

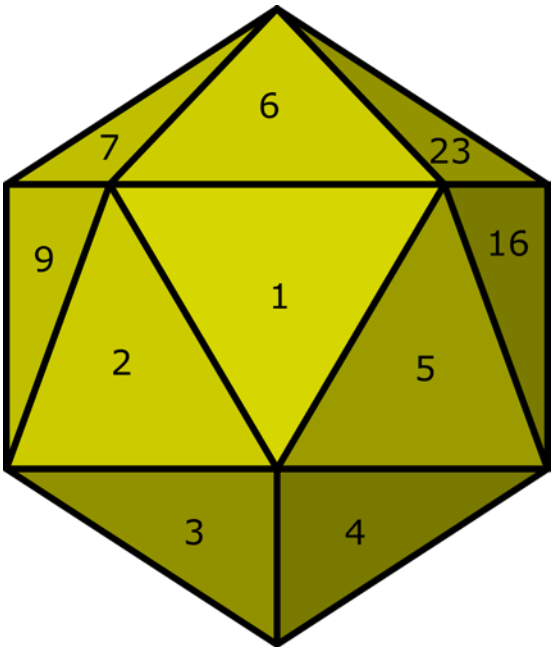

FIGURE 3

A numbered icosahedron showing all faces neighboring asymmetric unit 1. The problem that needed to be addressed for the algorithm to be successful is assigning these neighbors in the correct position for all 60 asymmetric units (i.e. – if we were to replace AU-1 with AU-40, which asymmetric units would go in place of AU-2, 3, 4, 5, 16, 23, 6, 7, and 9).

60 asymmetric units present in the capsid (Figure 3). A generalized algorithm to identify neighboring asymmetric units in the correct relative orientations. Each asymmetric unit (AU) is numbered (somewhat arbitrarily). First, we find neighbors of AU-1 by calculating pairwise distances between atoms composing AU-1 and those creating the rest of the capsid. If an AU has an atom within 12 Å of AU-1, it is considered a neighbor. Then we create a simplified representation of the capsid by representing each AU as a center of mass (COM) point, and an orientation basis. We transform the COM of each neighbor of AU-1 by the orientation basis of AU-1. This collection of vectors can now be used to find neighbors for all the other asymmetric units. Now, for each AU-x (where x is the AU number), we can transform the COMs of all AUs by the orientation basis of AU-x. Then the coordinates of the neighbor vectors will point to all the neighbors of AU-x. This approach allows us to not only find neighbors for each asymmetric unit, but also get them in the right relative positions. (i.e. if AU-1 has two neighbors AU-2 (on the left) and AU-3 (on the right), for any given AU, we know which neighbor is on the left and which is on the right). Once we know how the neighbors map to all the asymmetric units, we can create the CG model and define the native contacts for the entire capsid from transformations of the information from the Gō Model of the expanded asymmetric unit. During this process we also converted the

CHARMM parameter files to GROMACS ITP files for defining the custom force fields to be used for the Gō model. The total size of the capsid model was 89700 CG particles.

Modeling the Probe Tip

The probe tip was modeled as a hemisphere with a radium of ~9 nm with 550 identical 2kDa particles arranged in a cubic lattice with a distance of 1.5 nm between the particles. Adjacent particles in the lattice were bonded to each other, and movement is frozen in the x and y direction.

In-silico Indentation Simulations

The simulations were performed using the GROMACS simulation package version 4.5.5[24] using a Langevin integrator with 1 ps^{-1} friction factor, 10 fs time step at a constant temperature of 270 K. Non-bonded forces are computed for residue pairs as far as 33 Å apart, and data were saved at 100 ps intervals. The interaction between the virus and tip follows the 12-10 potential, where the interaction becomes repulsive at distances below 15 Å. The tip is moved by applying an umbrella potential with a spring constant of 200 kJ/(mol·$Å^2$) at a rate of 2×10^{-5} nm/ps. The force acting on the virus is determined from the difference between the location of umbrella potential and center of mass of the tip as shown in equation ,

$$F(t) = k(z(t) - z_0 - v \times t) \tag{4}$$

where z_0 is the initial tip center of mass position and v is the umbrella velocity.

We performed a total of nine nanoindentation simulations on the CG model of an NVLP. There were 3 trials for each of three orientations of the tip on the capsid: the tip was either on the two-fold, 3-fold, or 5-fold axis of the capsid. This was done to account for orientational averaging that occurs in experimental nanoindentations due to lack of control of viral particle adhesion to the slide. Additionally, the residues in the bottom half of the capsid were held in fixed positions to reduce

noise in the data. Furthermore, this serves to better replicate the experimental AFM indentations as the capsid has to be initially stuck to a slide which leads to deformation of the bottom half of the capsid.

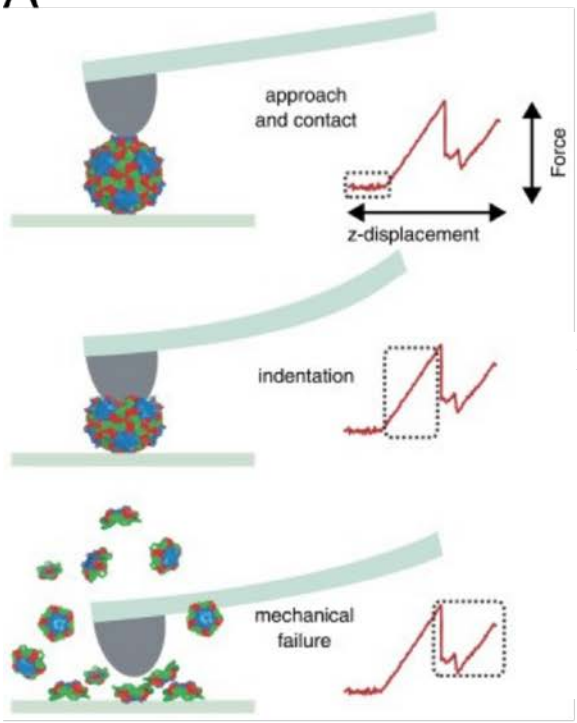

FIGURE 4

(A) Schematic of experimental ADM nanoindentation with force-indentation curves.

(B) Snapshots from a trajectory along a twofold symmetry axis. As the trajectory progresses, and the AFM tip pushes down, the distortion in the capsid can be seen. Because the bottom half is immobilized, it does not exhibit any deformation.

Calculating the Spring Constant, Critical Force, and Critical Indentation

The spring constant, k_c, relates the capsid stress and strain during the initial phase of deformation, where the capsid displays a linear elastic character. It is determined from the initial linear region of the force vs indentation curves.

The critical force signifies the maximum force the capsid can withstand before fracturing. The critical indentation is the indentation at which the critical force is observed. These values are determined from the point at which the force sharply decreases in the force vs indentation curves.

We computed the average mechanical properties by using a weighted average of the 3 orientations based on how often they occur in the viral capsid based on there being 30 twofold, 20 threefold, and 12 fivefold sites on an icosahedron capsid. Similarly, in order to calculate a standard deviation (SD), a distribution of the values was created by duplicating the measured values to match the ratio of values to the symmetry probabilities. This SD served as the errors for the means.

Evaluating the Relative Strengths of Protein-Protein Interfaces

The protein-protein interface strengths were evaluated based on the amount of time it took for the various types of interfaces to break. The interfaces were grouped by which version of the VP1 protein they were in between (A, B, or C), and were further distinguished by whether they were between the P domains or S domains. There was one additional distinction for interactions between the shell domains of the A and B subunits (SA-SB) in order to distinguish the dimer forming interface, and the non-dimer interface.

A residue pair was considered to be maintaining its contact while the distance between them was less than or equal to 1.5 times the native contact distance (as defined by the Gō model). When the distance in a simulation frame went higher than this value, the contact was defined as broken. A protein interface contact was defined as broken when at least 50% of the native contacts were lost

for the remaining trajectory. This analysis was performed using in-house software utilizing the Pteros 2.0 library[25].

Results and Discussion

Comparing the Simulated Mechanical Properties to the Experimental Values

The mechanical parameters we chose to focus on were the spring constant of the capsid, the maximum force the capsid could withstand (critical force), and the indentation depth at which the critical force occurred (critical indentation). These values allowed us to compare our simulation to the experimental AFM indentation by Baclayon et al.[9] in order to evaluate the relevance of the simulation to actual Norovirus capsid properties.

Our average spring constant is $k = 0.21 \pm 0.05$ N/m, which was in good agreement with the experimentally reported value of 0.30 ± 0.09 N/m,[9] the errors are SDs of the distribution. The SD of the simulation data is based on duplicating the measured values such that the ratios of values from the different symmetries are consistent with the ratio of those symmetries in the capsid. Our spring constants ranged from 0.12 to 0.26 N/m, while the experimental range was from 0.10 to 0.65 N/m. The high stiffness seen in the experimental data were low probability events, and it is likely that our nine simulations were not a large enough sample size to capture the full range. Despite this, our average spring constant is in exact agreement with the experimental data, and lends support to the validity of our model.

Our average critical force was $f_c = 1.6 \pm 0.2$ nN, and average critical indentation was $z_c = 6.8 \pm 0.7$ Å. The experimentally determined values are $f_c = 1.1 \pm 0.9$ nN and $z_c = 4.1 \pm 3.7$ Å[9]. Again,

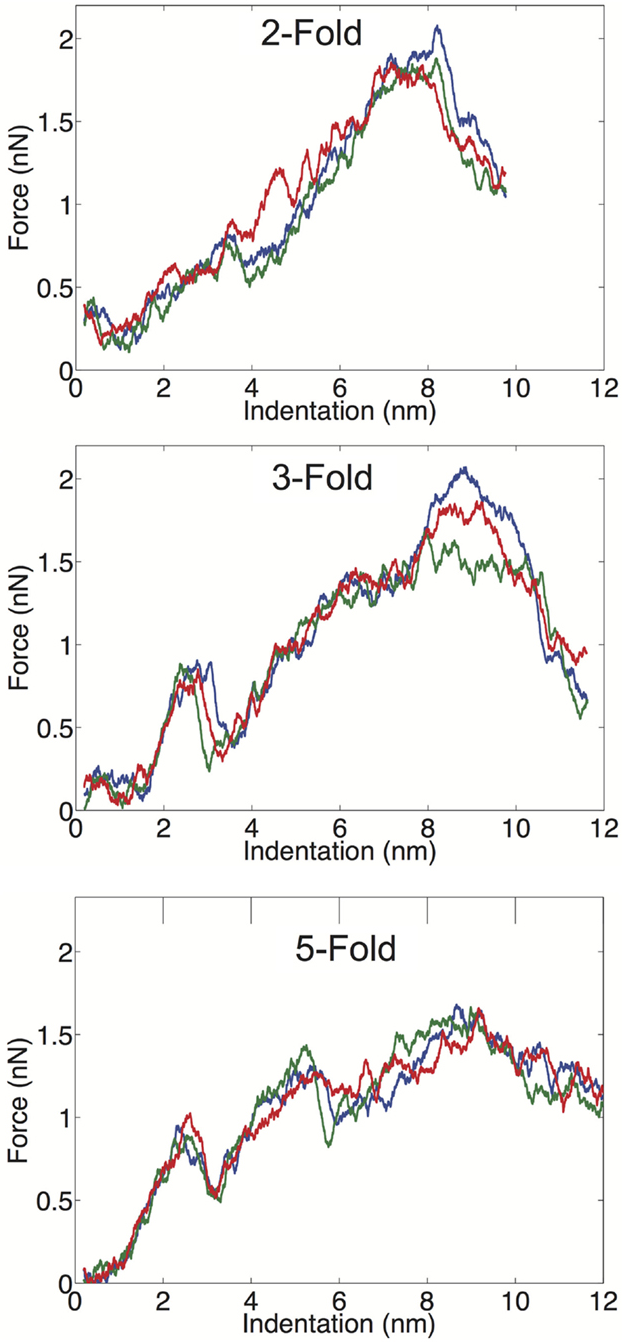

FIGURE 5

FZ curves along the twofold (top), threefold (middle), and fivefold (bottom) symmetry axes. Each line corresponds to one of three trials[31].

the errors are SDs of the distributions, and it can be seen that the simulated and experimental distributions overlap. The overestimation of these values most likely has to do with the high force loading rate applied to the tip in the simulation. The experimental loading rate of 50 nm/s is not feasible in MD even with a CG model because it would take too much computation time to get a simulation in which significant indentation has occured. MD nanoindentation simulations from previous studies have ranged from 10^4 nm/s[26] to 10^{10} nm/s[27]. Our loading rate of 10^7 nm/s was well within this range. These rates may appear extremely different, but it these are not true rates because the dynamics in CG models are accelerated due to a smoothed energy surface. It is likely that the effective dynamics from the Gō-like model is at least three orders of magnitude faster than the actual simulation time[28]. This would put our effective loading at 10^4 nm/s. While a slower loading rate in our simulations may improve the agreement in the calculated

mechanical properties, the overall model seems to perform well in comparison to the experimental indentation, and is adequate for addressing the relative strengths of the protein-protein interfaces.

Relative Strengths of Protein-Protein Interfaces

We tabulated the number of different interfaces broken throughout the simulation. The relative number of breaks accumulated by the different interfaces can be explained by the order in which capsid assembly proceeds. In solution, the VP1 protein forms dimers before capsid formation begins[8]. Accordingly, it would make sense that these are the strongest interactions. This might be

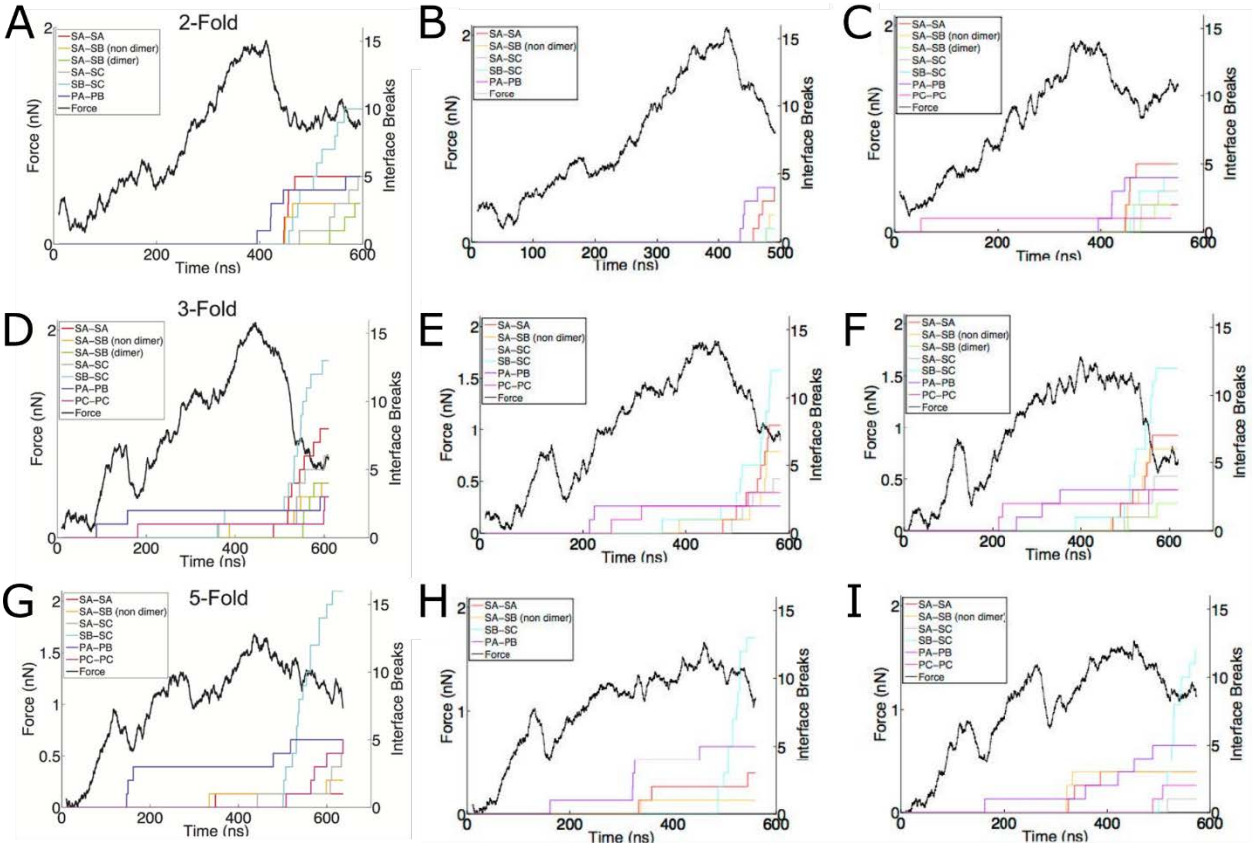

FIGURE 6

FT curves overlaid with the interface breaks during the simulation. All trials of indentation along the twofold (A-C), threefold (D-F), and fivefold (G-I) symmetry axes are shown. All interfaces, which accumulated at least two breaks, are shown. The colored lines represent the cumulative sum of the number of interfaces, which become broken, for various interface types. Interfaces are considered broken once the fraction of native contacts in that interface has dropped below 50% for a consecutive period of 5 ns[31].

explained by the larger interaction area for the dimer interaction because of their P domains interacting. Indeed, the A – B and C – C dimers generally accumulated the fewest breaks. In fact, the C – C dimers never accumulated breaks in any of the 9 simulations. This would suggest that the C – C dimers have a stronger interface than an A – B dimer. This might be due to the fact that the A – B dimer interface is slightly distorted in the capsid, whereas the C – C dimer conformation in the capsid is identical to the solution VP1 dimer. The additional strain in the A – B dimer may make it's interface weaker.

It is also known that a nucleation event must occur for dimer assembly into a complete capsid. Ion mass spectrometry experiments have shown that a pentamer of A – B dimers is the likely the assembly nucleus[29]. This would imply that the pentamer should be stronger than the hexamer. This is precisely what we observe in our analysis. The SA – SA interface that forms the pentamer breaks less often than the SB – SC interface that forms the hexamer. By and large, the SB – SC interfaces were clearly accumulating the most breaks in 8 of the 9 simulations.

Putative target sites for B–C interface stabilization

Because our analysis indicated that the B – C interface was the weakest protein interface in the capsid, we tried to identify binding hotspots across this interface that may serve as binding sites for an uncoating inhibiting antiviral. We used the FTMap server to identify these sites. It uses organic probe molecules to identify consensus binding sites on a protein surface[30]. We were able to run it just on the residues that are on the B – C interface, and isolate 3 binding sites that spanned the interface.

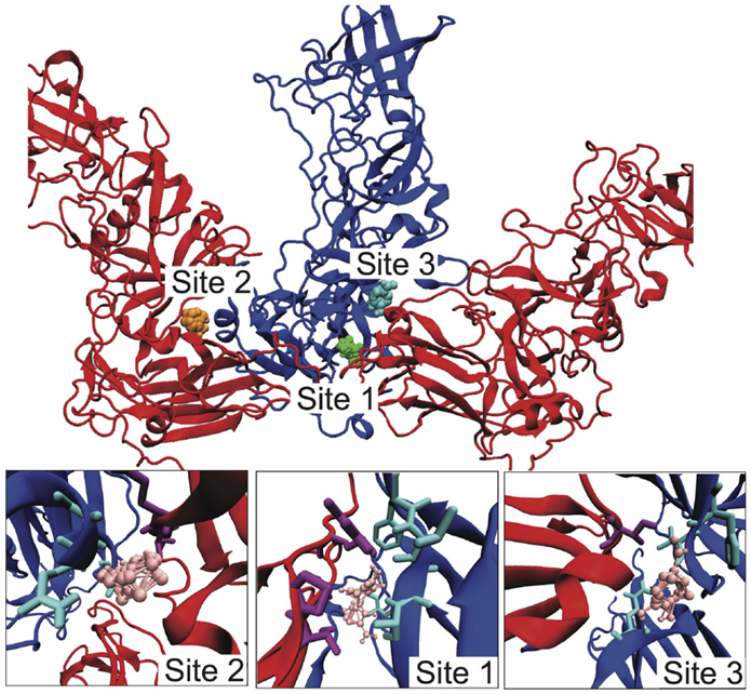

FIGURE 7

Identification of potential SB–SC stabilization sites. Using FTMap three binding sites were identified, which bound to residues in both subunits B and C. Subunit B is drawn in blue and subunit C is red. In the top image, the probes at site 1 are green, at site 2 orange, and site 3 cyan. In the lower zoom-in images, the organic probes are pink, residues with an atom within 3Å of a probe is drawn in as cyan for subunit B, and purple for subunit C[31].

TABLE 1

Target residues in the three putative binding sites to stabilize the B – C interface[31]

Binding site	**Subunit B residues**	**Subunit C residues**
1	ALA114, PHE200, VAL201, VAL202, ALA203	GLY121, THR188, PRO189, ARG191
2	ALA140, GLN141, LEU144	VAL61, GLN62
3	GLN62, PHE503, VAL504	THR130

Conclusion

Our *in-silico* coarse grained nanoindentation simulations were able to reproduce several mechanical properties of the Norwalk virus capsid, and give further insight into capsid dynamics that could not have been revealed through experimental techniques alone. We were able to tabulate the relative strengths of the protein-protein interfaces in the capsid. These strengths were consistent with the known intermediates in capsid formation. Furthermore, we saw a clearly weak interface in the capsid

between the B – C subunits. The separation of this surface might serve as the activation event for viral uncoating, though further experimentation is needed to confirm this hypothesis. If this is indeed the case, a drug that can bind and strengthen this interface would be a promising antiviral compound. Accordingly, we used FTMap to identify three sites that a potential small molecule may attempt to bind in order to strengthen this interface.

References

1. Bertolotti-Ciarlet, A., White, L. J., Chen, R., Prasad, B. V. V. & Estes, M. K. Structural requirements for the assembly of Norwalk virus-like particles. *J. Virol.* **76,** 4044–4055 (2002).

2. Iturriza-Gómara, M. & Lopman, B. Norovirus in healthcare settings. *Curr. Opin. Infect. Dis.* **27,** 437–43 (2014).

3. Lopman, B. A., Steele, D., Kirkwood, C. D. & Parashar, U. D. The Vast and Varied Global Burden of Norovirus: Prospects for Prevention and Control. *PLoS Med.* **13,** e1001999 (2016).

4. Hall, A. J. *et al.* Norovirus disease in the United States. *Emerg. Infect. Dis.* **19,** 1198–205 (2013).

5. Lopman, B. *et al. Global burden of norovirus and prospects for vaccine development. Centers for Disease Control and Prevention* (2015).

6. Boyd, K. J., Bansal, P., Feng, J. & May, E. R. Stability of Norwalk Virus Capsid Protein Interfaces Evaluated by in Silico Nanoindentation. *Front. Bioeng. Biotechnol.* **3,** 1–8 (2015).

7. Bull, R. a, Eden, J.-S., Rawlinson, W. D. & White, P. a. Rapid evolution of pandemic noroviruses of the GII.4 lineage. *PLoS Pathog.* **6,** e1000831 (2010).

8. Prasad, B. V. V. X-ray Crystallographic Structure of the Norwalk Virus Capsid. *Science (80-.).* **286,** 287–290 (1999).

9. Baclayon, M. *et al.* Prestress strengthens the shell of norwalk virus nanoparticles. *Nano Lett.* **11,** 4865–4869 (2011).

10. Katpally, U., Wobus, C. E., Dryden, K., Virgin, H. W. & Smith, T. J. Structure of antibody-neutralized murine norovirus and unexpected differences from viruslike particles. *J. Virol.* **82,** 2079–88 (2008).

11. Katpally, U. *et al.* High-resolution cryo-electron microscopy structures of murine norovirus 1 and rabbit hemorrhagic disease virus reveal marked flexibility in the receptor binding domains. *J. Virol.* **84,** 5836–41 (2010).

12. CASPAR, D. L. & KLUG, A. Physical principles in the construction of regular viruses. *Cold Spring Harb. Symp. Quant. Biol.* **27,** 1–24 (1962).

13. Perry, J. W. & Wobus, C. E. Endocytosis of murine norovirus 1 into murine macrophages is dependent on dynamin II and cholesterol. *J. Virol.* **84,** 6163–76 (2010).

14. Roos, W. H., Bruinsma, R. & Wuite, G. J. L. Physical virology. *Nat. Phys.* **6,** 733–743 (2010).

15. Cuellar, J. L., Meinhoevel, F., Hoehne, M. & Donath, E. Size and mechanical stability of norovirus capsids depend on pH: a nanoindentation study. *J. Gen. Virol.* **91,** 2449–56 (2010).

16. Cieplak, M. & Robbins, M. O. Nanoindentation of 35 virus capsids in a molecular model: relating mechanical properties to structure. *PLoS One* **8,** e63640 (2013).

17. Mckinlay, M. A., Pevear, D. C., York, N. & Rossmann, M. G. Treatment of the picornavirus common cold by inhibitors or viral uncoating and attachment. *Annu. Rev. Microbiol.* **46,** 635–54 (1992).

18. Karplus, M. & McCammon, J. A. Molecular dynamics simulations of biomolecules. *Nat. Struct. Biol.* **9,** 646–652 (2002).

19. Wang, Y. & Mccammon, J. A. Computational Modeling of Biological Systems. (2012). doi:10.1007/978-1-4614-2146-7

20. Weiner, P. K. & Kollman, P. a. AMBER: Assisted model building with energy refinement. A general program for modeling molecules and their interactions. *J. Comput. Chem.* **2,** 287–303

(1981).

21. Vanommeslaeghe, K. *et al.* CHARMM general force field: A force field for drug-like molecules compatible with the CHARMM all-atom additive biological force fields. *J. Comput. Chem.* **31,** 671–690 (2010).

22. Schmid, N. *et al.* Definition and testing of the GROMOS force-field versions 54A7 and 54B7. *Eur. Biophys. J.* **40,** 843–856 (2011).

23. Jorgensen, W. L. & Tirado-Rives, J. The OPLS [optimized potentials for liquid simulations] potential functions for proteins, energy minimizations for crystals of cyclic peptides and crambin. *J. Am. Chem. Soc.* **110,** 1657–1666 (1988).

24. Van Der Spoel, D. *et al.* GROMACS: fast, flexible, and free. *J. Comput. Chem.* **26,** 1701–18 (2005).

25. Yesylevskyy, S. O. Pteros: Fast and easy to use open-source C++ library for molecular analysis. *J. Comput. Chem.* **33,** 1632–1636 (2012).

26. Kononova, O. *et al.* Structural transitions and energy landscape for Cowpea Chlorotic Mottle Virus capsid mechanics from nanomanipulation in vitro and in silico. *Biophys. J.* **105,** 1893–903 (2013).

27. Zink, M. & Grubmüller, H. Mechanical properties of the icosahedral shell of southern bean mosaic virus: a molecular dynamics study. *Biophys. J.* **96,** 1350–63 (2009).

28. Buck, P. M. & Bystroff, C. Constraining local structure can speed up folding by promoting structural polarization of the folding pathway. *Protein Sci.* **20,** 959–69 (2011).

29. Uetrecht, C., Barbu, I. M., Shoemaker, G. K., van Duijn, E. & Heck, A. J. R. Interrogating

viral capsid assembly with ion mobility-mass spectrometry. *Nat. Chem.* **3,** 126–32 (2011).

30. Brenke, R. *et al.* Fragment-based identification of druggable 'hot spots' of proteins using Fourier domain correlation techniques. *Bioinformatics* **25,** 621–7 (2009).

31. Boyd, K. J., Bansal, P., Feng, J. & May, E. R. Stability of Norwalk Virus Capsid Protein Interfaces Evaluated by in Silico Nanoindentation. *Front. Bioeng. Biotechnol.* **3,** (2015).